J Food Sci Technol (April 2019) 56(4):1829–1840
https://doi.org/10.1007/s13197-019-03635-7

ORIGINAL ARTICLE

Development of electrochemical biosensor based on CNT–Fe_3O_4 nanocomposite to determine formaldehyde adulteration in orange juice

Monika Kundu[1,2,3] · Hema Bhardwaj[2,3] · Manoj Kumar Pandey[2] · Prameela Krishnan[1] · R. K. Kotnala[2] · Gajjala Sumana[2,3]

Revised: 21 January 2019 / Accepted: 3 February 2019 / Published online: 18 February 2019

Abstract An electrochemical biosensor was developed to determine formaldehyde (HCHO) adulteration commonly found in food. The current responses of various electrodes based on multiwalled carbon nanotubes (CNTs) and synthesized nanocomposite (CNT–Fe_3O_4) were measured using cyclic voltammetry. The nanocomposite based biosensor shows comparatively high sensitivity (527 μA mg/L^{-1} cm^{-2}), low detection limit (0.05 mg/L) in linear detection range 0.05–0.5 mg/L for formaldehyde detection using formaldehyde dehydrogenase (FDH) enzyme. In real sample analysis, the low obtained RSD values (less than 1.79) and good recovery rates (more than 90%) signify an efficient and precise sensor for the selective quantification of formaldehyde in orange juice. The developed biosensor has future implications for determining formaldehyde adulteration in citrus fruit juices and other liquid foods in agri-food chain to further resolve global food safety concerns, control unethical business practices of adulteration and reduce the widespread food borne illness outbreaks.

Keywords Iron oxide · Multiwalled carbon nanotubes · Nanocomposite · Orange juice · Formaldehyde

Introduction

In the modern world, fast moving civilization has led to continuous addition of lot of venomous elements in the environment. There are ever increasing cases of food toxicity and reported deaths (Nedellec et al. 2016). Food directly influences our health and ultimately the growth and development of a nation. In agriculture, one of the major aspects of food safety is adulteration which is of prime concern for whole of the world today. Among various malpractices of using adulteration in food, formaldehyde adulteration is found to be very common globally and the developing countries are the worst sufferers. Formaldehyde is commonly used as formalin (37% formaldehyde) in various labs and industries. Besides its use as an antiseptic, formalin inactivates most of the bacteria and fungi. It is used in aquaculture treatments for killing parasites (protozoans, monogenetic tremetodes etc.) found on fish body. Formaldehyde is very often used for preservation of biological specimens, cosmetics and food products (European Food Safety Authority 2007). The malpractice of using preservatives such as formaldehyde for enhancing shelf life has been reported at many places all over the world in food such as milk (Ahmed et al. 2015), seafood (Goon et al. 2014) and fruits and vegetables (Wahed et al. 2016). Rapid detection of this chemical is essential due to its carcinogenicity, persistence and stability. A high dose of formalin in our body can cause diarrhoea, vomiting and even gastrointestinal tract ulcer. When inhaled in excess as a gas, it may cause asthma, pulmonary edema and may increase the rate of respiratory cancer and also affects the reproductive

Electronic supplementary material The online version of this article (https://doi.org/10.1007/s13197-019-03635-7) contains supplementary material, which is available to authorized users.

✉ Gajjala Sumana
sumanagajjala@gmail.com

[1] Division of Agricultural Physics, ICAR-Indian Agricultural Research Institute, New Delhi 110012, India

[2] CSIR-National Physical Laboratory, Dr. K.S. Krishnan Marg, New Delhi 110012, India

[3] AcSIR-CSIR-National Physical Laboratory, Dr. K.S. Krishnan Marg, New Delhi 110012, India

health and causes dermatitis (Goon et al. 2014). Due to these lethal health effects an International Agency for promoting Research on Caner (IARC) has categorized formaldehyde in Group 1 carcinogen to human beings (World Health 2004). US Food and Drug Administration (USFDA) identifies formaldehyde for use only as a component of adhesives and does not recommend its use in human food (Wahed et al. 2016). For the quantitative analysis of formaldehyde in samples, various existing techniques such as HPLC (Jeong et al. 2015), gas chromatography (Zhang et al. 2015) and chemiluminescence (Khataee et al. 2016) are used in laboratory. As established, most of these chemical methods are long, expensive, laborious and require skilled personnel to carry out the testing and run the instrumentation. Thus, there is need of rapid, sensitive, portable and low cost technology to determine formaldehyde adulteration in food. In this regard a formaldehyde sensor is urgently needed. Researches all over the world have established various innovative methods and techniques for providing enlightening solutions to this problem. In this regard, available chemical kits are less reliable due to accuracy and non specificity reasons (Kumar et al. 2015). These are suitable only for obtaining first hand information at lab scale. Very few studies have been conducted in the field of fabrication of biosensors for quantification of food adulterants such as formaldehyde in fruit juices. Among the reported studies most of them are focused on study of naturally occurring formaldehyde content in fish and seafood. A formaldehyde biosensor based on differential pulse voltammetry method has been reported for formalin detection in fish based on gold nanoparticles based matrix (Noor Aini et al. 2016). Among the dairy products, the concentration of formalin as preservative in cow milk has been studied using spectrometric technique. With optical and statistical analysis for varying concentrations of formalin in milk, a laboratory scale formalin adulteration analysis method has been established (Mabood et al. 2017). A potentiometric biosensor has been developed for formaldehyde detection using alcohol oxidase and pH-sensitive transducer in linear range of 5–200 mM (Korpan et al. 2000). Thus, non-availability of biosensors for the formaldehyde determination in fruits and vegetables is a serious concern demanding immediate focus on development of formaldehyde biosensor. In this context, iron oxides nanostructures possess multifunctional properties such as: (1) large surface area, (2) good biocompatibility, (3) nontoxicity, (4) chemical stability, (5) accelerated electron transport behaviour and (6) controlled particle size. Use of such nanomaterials can lead to improved electrocatalytic activity of the biomolecule and better sensitivity for detection of target analyte (Sharma et al. 2013). Keeping all this in view, a nanocomposite of CNT and iron oxide (Fe_3O_4) was synthesized and used as a matrix for the development of a biosensor.

Thus, in view of the existing research gaps, we are reporting for the first time, a formaldehyde biosensor for detection of orange juice adulteration based on CNT–Fe_3O_4 nanocomposite and developed using cyclic voltammetry (CV). Further, efforts have been made to probe into mechanisms of interactions of formaldehyde dehydrogenase (FDH) with formaldehyde at interfaces with carboxyl-functionalized CNT, CNT–Fe_3O_4 nanocomposite and co-enzyme (NADH). The developed matrix can be used for real sample analysis in citrus juices and other liquid foods.

Experimental section

Materials and reagents

Multiwalled carbon nanotubes (CNT) (90%), acetonitrile, magnesium nitrate ($Mg(NO_3)_2$), sulphuric acid, nitric acid, β-Nicotinamide adenine dinucleotide (NADH), bovine serum albumin (BSA), formaldehyde dehydrogenase from *Pseudomonas* sp. (FDH), N-Hydroxysuccinimide (NHS), N-ethyl-N′-(3-dimethylaminopropyl carbodiimide) (EDC), ferric chloride hexahydrate ($FeCl_3.6H_2O$), ferrous sulphate heptahydrate ($FeSO_4.7H_2O$), ammonia (NH_4OH, 25%) and formaldehyde (HCHO) were purchased from Sigma-Aldrich, USA. Glass slides coated with indium tin oxide (ITO) (sheet resistance, 40–60 Ω sq^{-1}) were used for electrophoretic deposition and further electrode fabrication. Distilled water (DI) (Milli-Q, Millipore, resistivity 18.2 MΩ cm) was used for preparation of all aqueous solutions in the study. Phosphate buffer and phosphate buffered saline (50 mM) at pH 7.4 containing 5 mM of $[Fe(CN)_6]^{3-/4-}$ ions and 0.9% NaCl solution were prepared. The different concentrations of formaldehyde from the stock solutions were prepared freshly in distilled water.

Instruments

To study the crystallite phase and structure of the synthesized nanoparticles, the X-ray diffraction studies were conducted using a diffractometer (Rigaku Corporation) with CuKα (1.5406 Å) radiation source within 10°–80° range of 2θ scale at room temperature. The X-ray diffraction (XRD) peaks positions for dried iron oxide nanoparticles were found to be consistent with the standard pattern for JCPDS 65-3107 (Han et al. 2014; Hariani et al. 2013). Spectroscopic characterization studies were conducted using UV–Vis spectrophotometer (UV–Vis, Lambda 950, Perkin Elmer, USA) and Fourier transform infrared spectrophotometer (FT-IR, Varian 660, Perkin Elmer). Morphological investigations of synthesized

nanoparticles and composite were accomplished using JEM 1011, JEOL (USA) transmission electron microscope (TEM) and scanning electron microscope (SEM, LEO 440). For studying electrochemical characteristics, Auto lab Potentiostat/Galvanostat from Eco Chemie, Netherland, equipped with three electrode configuration in a conventional cell designed with electrodes of Ag/AgCl and platinum foil (Pt) as reference and counter probes respectively was used. PBS (50 mM) at pH 7.4, consisting of ferrocyanide-ferricyanide (5 mM) redox couple was used as the electrolyte in the electrochemical cell.

Functionalization of CNT

For the functionalization and purification of carbon nanotubes (90%) the boiling acid treatment method was used. In this method, carbon nanotubes were continuously refluxed with sulphuric acid (98%, w/v) for 12–13 h, and then rinsed with DI. Afterwards as obtained CNTs were rinsed properly with ethanol and finally dried at 60 °C in microwave oven (Das et al. 2012).

Synthesis of iron oxide (Fe_3O_4) nanoparticles

Well dispersible nanoparticles of Fe_3O_4 have been synthesized via chemical coprecipitation method (Kulkarni et al. 2014). The solution of ferric chloride hexahydrate ($FeCl_3{\cdot}6H_2O$) and ferrous sulphate ($FeSO_4{\cdot}7H_2O$) in distilled water was prepared by dissolving in 2:1 molar ratio. Few drops of concentrated HCl were added to this solution for complete dissolution of iron salts and was further heated up to 323 K for 1200 s. The prepared solution was added slowly into ammonia (NH_4OH, 25%) solution till the pH reached 11–12 under vigorous stirring (Kang et al. 1996). As a result of this, black precipitates of Fe_3O_4 started generating in the solution. After the completion of the reaction, the suspension was allowed to cool, and later separated by centrifugation at 3000 r.p.m. for 600 s. Then the decantation was done and the obtained magnetic nanoparticles were repeatedly washed in distilled water. They were then dried in microwave oven at temperature of 353 K for 10,800 s.

Synthesis of CNT–Fe_3O_4 nanocomposite

For synthesis of nanocomposite, functionalized CNT and Fe_3O_4 nanoparticles were dispersed in optimized ratio (1:2, w/w) in a mixture of ethanol-distilled water (2:1, v/v). The solution was then kept on magnetic stirrer at 333 K for 21,600 s (Fayemi et al. 2017). From UV–Vis spectra, the formation of nanocomposite was confirmed by the absorption band shifts obtained.

Preparation of orange juice samples

Fresh oranges (*Citrus reticulata* Blanco) were collected from the local fruit market, New Delhi city, India. The juice was extracted by manual pressing of the edible part of the oranges and further used for the analysis. Along with this, commercialized orange juice was also analyzed. The sample preparation procedure followed the previously reported method (Razzino et al. 2015). The formaldehyde concentration was determined in orange juice samples with optimized dilutions (5.0% (v/v) in PBS (pH 7.4) incorporating $[Fe(CN)_6]^{3-/4-}$ (5 mM). Using cyclic voltammetry (CV) the current response of various bioelectrodes was studied with the variation in formaldehyde concentration in juices (Ding et al. 2016). The recovery rates and RSD values were calculated for both types of juices using two different bioelectrodes based on CNT and CNT–Fe_3O_4 nanocomposite.

Electrophoretic deposition

The electrophoretic deposition technique (EPD) was used to deposit CNT and nanocomposite (CNT–Fe_3O_4) material on to indium tin oxide (ITO) coated glass electrode during fabrication of electrodes (Dhyani et al. 2012). Before any deposition, ITO coated glass electrodes (2×1 cm^2) were precleaned by hydrolyzation with solution consisting of 1:1:5 (v/v) ratio of $H_2O_2/NH_4OH/H_2O$ respectively at 353 K for 1800 s. For preparing the dispersion of CNT–Fe_3O_4 (50 mg/dl), a mixture of ethanol–water (2:1) was used as a solvent and the obtained suspension was ultrasonicated (50 W, 0.25 A) continuously for 14,400 s (Sharma et al. 2013). Using this dispersion, suitable colloidal suspension for EPD was prepared. The EPD set-up consisted of a constant and regulated DC voltage as power source and two electrodes. Hydrolyzed ITO glass substrate along with platinum foil served as anode and cathode respectively. The two electrode system was then inserted into the colloidal solution of CNT–Fe_3O_4 nanocomposite and optimized constant voltage of 15 V was applied for 120 s for obtaining uniform monolayer deposition onto ITO substrate. After removing from the suspension the CNT–Fe_3O_4/ITO electrodes were then rinsed with distilled water and further dried at room temperature (298 K). Similarly for fabricating CNT/ITO electrodes, CNT dispersion (50 mg/dl) in acetonitrile was prepared. In the colloidal suspension small concentrations of magnesium nitrate ($Mg(NO_3)_2{\cdot}6H_2O$) was added to create surface charge on CNT. The obtained suspension was ultrasonicated for about 10,800 s and then used for EPD to get CNT/ITO electrodes (Singh et al. 2013).

Immobilization of enzyme onto CNT/ITO and CNT–Fe_3O_4/ITO electrodes

Prior to immobilization of enzyme, EDC: NHS chemistry was used for activation of CNT/ITO and CNT–Fe_3O_4/ITO electrodes. In this combination, EDC performed as the coupling agent for proper immobilization of enzyme and NHS as the activator. EDC and NHS solutions with concentrations of 0.2 M and 0.05 M were prepared and mixed in 1:1 ratio. 10 µl of this formulated solution was then applied on to the electrodes by drop cast method to activate the carboxylic groups on the CNT/ITO and CNT–Fe_3O_4/ITO electrodes. The EDC:NHS coated electrodes were then stored in refrigerator at 4 °C for 3 h. A suitable optimized concentration (10 µg/mL) of enzyme in PB (pH 7.4) was used as stock solution of enzyme for further application. The enzyme solution (10 µL) was applied evenly on CNT/ITO and CNT–Fe_3O_4/ITO electrodes that had been already activated via EDC:NHS chemistry (Fig. 1). The amine groups of FDH enzyme are bound covalently to carboxyl group of CNT–Fe_3O_4 through strong amide bonds (CO–NH) (Fischer 2010). These electrodes were then incubated under humid chamber at room temperature for 6 h. After incubation, the electrodes (FDH/CNT/ITO and FDH/CNT–Fe_3O_4/ITO) were then treated with bovine serum albumin (BSA) solution (1 mg/mL) to cover the non-specific sites present on the surface (Bhardwaj et al. 2016). These bio-electrodes (BSA/FDH/CNT/ITO and BSA/FDH/CNT–Fe_3O_4/ITO) were then rinsed in PBS and stored in refrigerator (4 °C) till further use.

Results and discussion

Spectroscopic and structural characterization of fabricated electrodes

UV–visible absorption spectrum of CNT, Fe_3O_4 nanoparticles and CNT–Fe_3O_4 nanocomposite are shown in Fig. 2a. In absorbance spectrum of CNT, the absorption peak region obtained at 250 nm indicated electronic transitions of C–C bonds in CNT. In the absorption spectrum of Fe_3O_4 nanoparticle, sample broad absorption peak ranging from 320 to 400 nm originated mainly from the optical properties (absorption and scattering of light) of magnetic nanoparticles. The band around 300 nm represented the ligand field transitions of Fe^{3+} and the peak around 375 nm depicted excitations of the Fe–Fe pair (Sherman and Waite 1985). The high absorption peak at 375 nm also indicated the formation of least agglomerated nanoparticles. In the CNT–Fe_3O_4 nanocomposite, a shifted absorption peak was observed at 260 nm due to absorption bands of Fe_3O_4 and CNT. Also a reduction in the Fe_3O_4 band intensity and enhancement of band intensity of CNT indicated the formation of CNT–Fe_3O_4 nanocomposite. The observed UV absorption ability of CNT–Fe_3O_4 nanocomposite was lesser as compared to the band intensity of the Fe_3O_4 nanoparticles but higher than that of CNT.

Furthermore, FT-IR spectrum of CNT/ITO, Fe_3O_4 nanoparticles, CNT–Fe_3O_4/ITO and FDH/CNT–Fe_3O_4/ITO were obtained as shown in Fig. 2b. The broad peak observed at 3265 cm^{-1} in all the curves was indicating the stretching of hydroxyl group (O–H) of adsorbed water

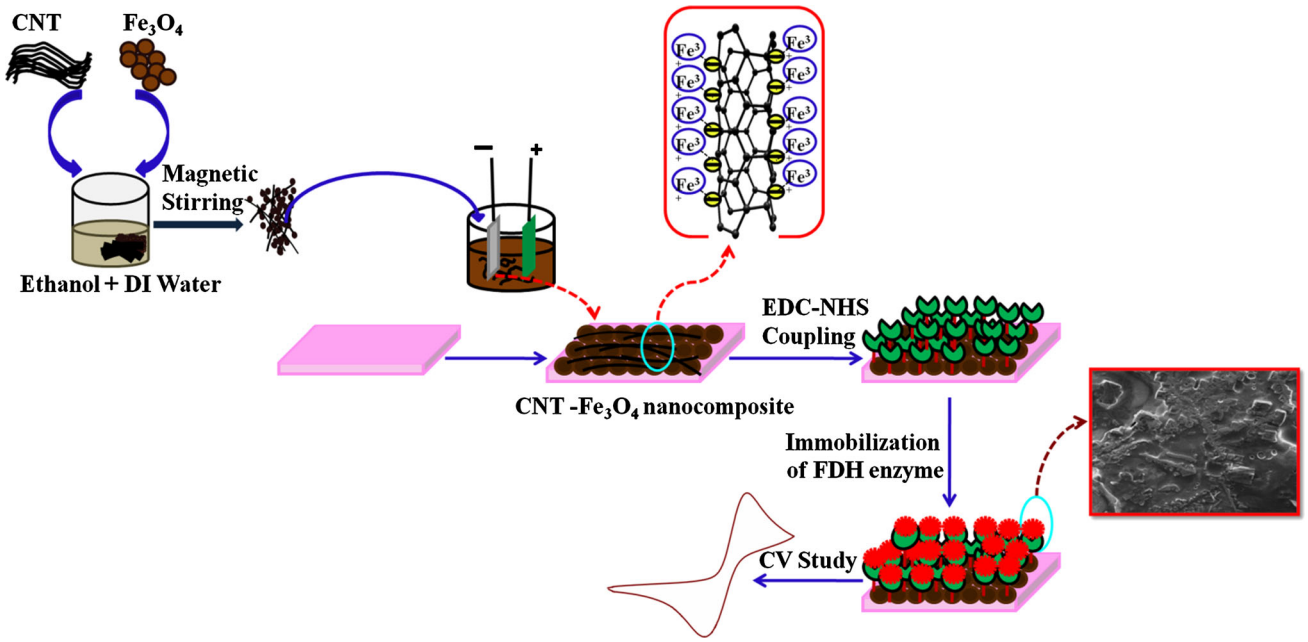

Fig. 1 Schematic representing fabrication of CNT–Fe_3O_4 nanocomposite based biosensor

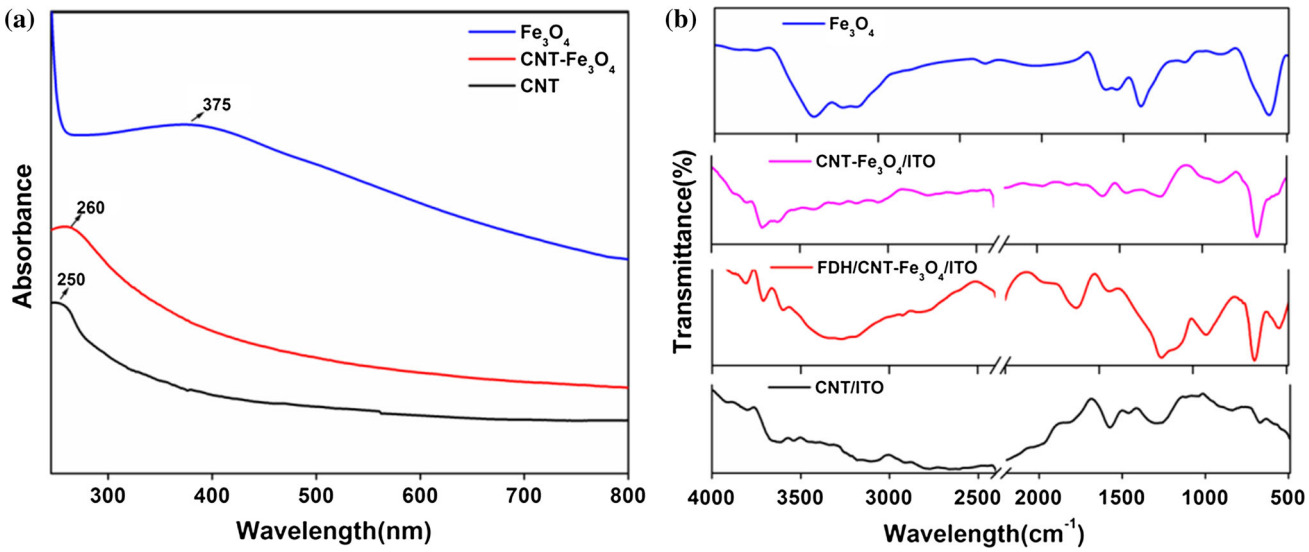

Fig. 2 **a** UV–visible absorption spectrum of synthesized nanoparticles, **b** FTIR spectrum of CNT, Fe_3O_4, CNT–Fe_3O_4 and immobilized CNT–Fe_3O_4 electrodes

molecules and absorption peak at 2357 cm^{-1} indicated presence of CO_2. The peak at 1260 cm^{-1} revealed stretching in bond C–O in CNT. Another peak around 1577 cm^{-1} pointed towards C=C bond stretching of graphite in CNT. Bands around 2808 cm^{-1} and 1458 cm^{-1} were due to asymmetric and symmetric stretching of C–H bonds in the CNTs (Singh et al. 2013). In spectrum, the high intense peak, sharply defined at 614 cm^{-1} reflected the high degree of crystallinity found in synthesized Fe_3O_4 nanoparticles (Fayemi et al. 2017). This peak pointed out the presence of Fe–O bond vibrations in the nanocomposite, and further confirms the presence of spinel structure of Fe_3O_4 nanoparticles. After immobilization some additional peaks, due to enzyme amide bonds, also appeared in the spectra of FDH/CNT–Fe_3O_4/ITO electrode. These might be perhaps due to the complex formation between the CNT–Fe_3O_4 and enzyme. This was highlighted by the observed reduction in intensities of major peaks. Absorption peaks arising at 1590 cm^{-1} and a doublet at 3537 cm^{-1} revealed bending and stretching vibrations of N–H band showing immobilization of enzyme on to the film.

In the XRD spectra of CNT (Fig. S1a), a sharply defined intense peak identified at 25.1° was due to (002) reflection plane and indicated the tubular structure of CNT. Another prominent diffraction peaks found at 43° represents (100) plane. The interplanar spacing for (002) plane of CNT was estimated as 0.35 nm. While in the XRD spectra of Fe_3O_4 nanoparticles (Fig S1b), face centered cubic spinel structure of the crystallite was obtained with formation of strongest reflection from the (311) plane. The sample showed very broad peaks, indicating the small crystallite size and ultrafine nature of the particles. Major diffraction peaks corresponding to planes (311), (440), (220), (511) and (422) indicated a cubic crystal structure for the Fe_3O_4 nanoparticles (JCPDS 65-3107) (Han et al. 2014; Zhu et al. 2016). It was evident from the XRD pattern that Fe_3O_4 particles were not contaminated by any foreign materials. The interplanar spacing was found to be 0.25 nm for the (311) plane. Further by using the Scherrer equation, crystallite size was also estimated. In our work the crystallite size for Fe_3O_4 nanoparticles was found to be 14 nm.

Morphological characterization

SEM images of CNT and CNT–Fe_3O_4 nanocomposite were recorded and indicates that the carbon nanotubes were loosely scattered tubular shaped particles. The thread like network represented the structure of carbon nanotube material (Fig. 3a). The SEM image of nanocomposite depicted intertwined complex network of carbon nanotubes with iron oxides nanoparticle clusters attached to them. At some places the agglomerations of iron oxide nanoparticles could be seen upon deposition due to their surface roughness (Fig. 3a). Since maximum gradient in electrical double layer existed at edges of nanoparticles, more and more nanoparticles are attracted towards each other due to electrostatic force among them. This caused agglomeration and led to growth in their size (Pramod et al. 2007). After immobilization of the CNT/ITO and CNT–Fe_3O_4/ITO electrodes, the dense uniform distribution of nanostructures was transformed to regular globular structures due to physical adsorption of formaldehyde dehydrogenase molecules onto CNT and nanocomposite films.

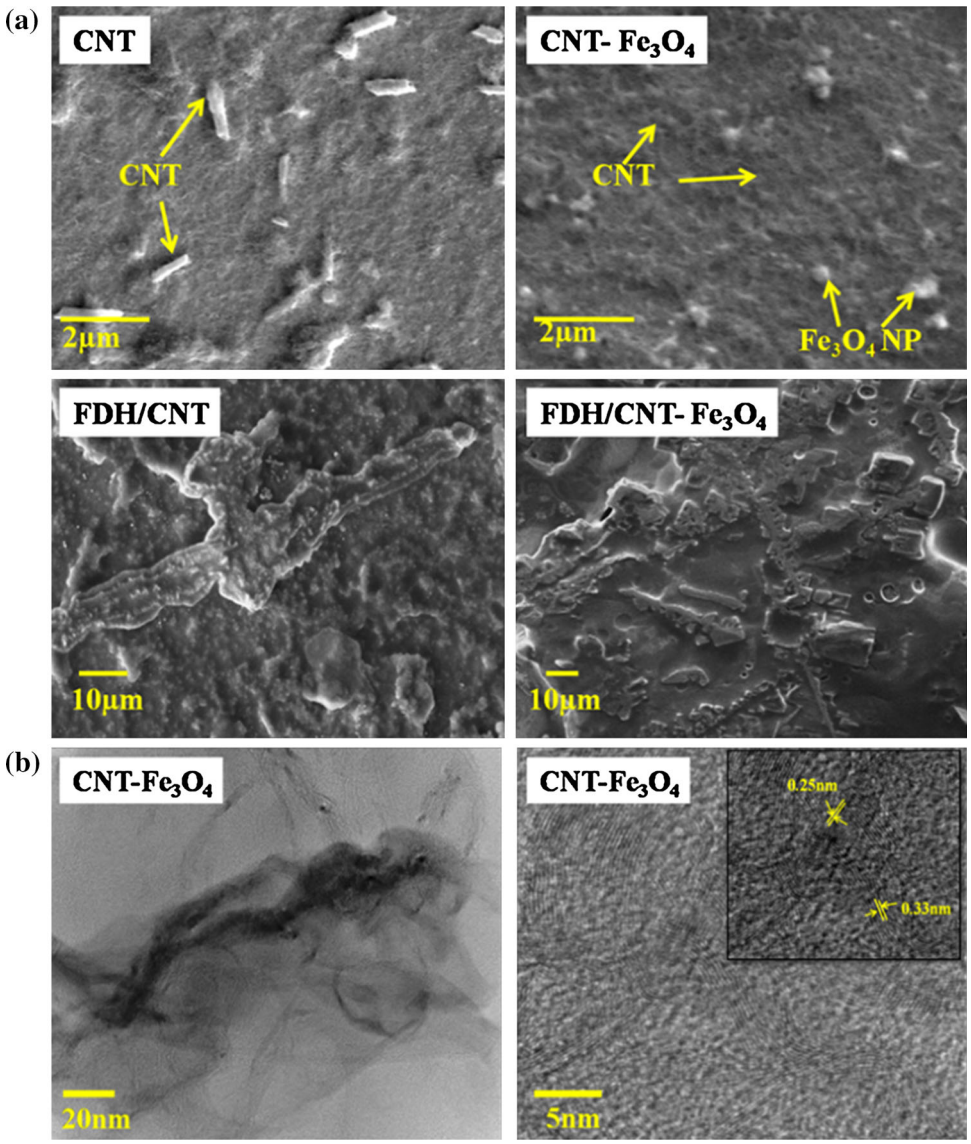

Fig. 3 **a** SEM images of different fabricated electrodes, **b** TEM images of CNT–Fe_3O_4 nanocomposite at 20 nm and 5 nm (inset: HR-TEM of CNT–Fe_3O_4 nanocomposite)

Figure 3b shows TEM images of CNT–Fe_3O_4 nanocomposite. CNT appeared to be well dispersed while metal oxide nanoparticles were seen attached on the length of nanotubes. Fe_3O_4 nanoparticles were of round or spherical structure. The high resolution electron microscopy (HR-TEM) image of nanocomposite with lattice fringes of CNT and Fe_3O_4 nanoparticles has been represented in Fig. 3b inset. The interplanar spacing was found to be 0.25 nm for (311) plane of Fe_3O_4 nanoparticles and 0.33 nm for (002) plane of CNT (Paul Joseph et al. 2010). The average diameter of CNT, as revealed from the images, was about 40–80 nm and length was about few microns whereas average size of Fe_3O_4 nanoparticles was about 10–15 nm that was found to be comparable with the XRD data also.

Electrochemical characterization

In the nanocomposite, CNT and Fe_3O_4 mixed in different ratios of 1:1 (w/w), 1:2 (w/w) and 1:3 (w/w) were studied using cyclic voltammetry (CV). The peak current increased as the concentration of Fe_3O_4 nanoparticles was increased in the composite, up to 1:2 ratio; afterwards the peak current showed a decreasing trend (Fig. S2). These findings of results revealed that by changing the Fe_3O_4 nanoparticle concentration there might be possibility of agglomeration and resulting oxide layer of Fe_3O_4 NPs caused hindrance, which obstructed the charge transfer in redox probe. Hence, the present study was carried out with optimized composition (1:2) of CNT–Fe_3O_4 nanocomposite. Furthermore, the electrochemical characterization of CNT/ITO, CNT–Fe_3O_4/ITO, FDH/CNT/ITO and FDH/CNT–Fe_3O_4/ITO electrodes was conducted using CV. In

addition, the underlying electron reaction kinetics, resistive hindrance encountered and double layer capacitance were studied by using electrochemical impedance spectroscopy (EIS). Peak current of CNT/ITO electrode was found to be higher than ITO glass electrode due to presence of structural defects in MWCNT. These defects influenced the electronic properties of the electrode by allowing electron transfer towards the electrode in the electrolyte (Fig S4a). The oxidation peak for CNT/ITO was obtained at 647.3 μA, while for CNT–Fe_3O_4/ITO the peak was obtained at 683.2 μA. Due to faster charge transport behavior of CNT–Fe_3O_4/ITO electrode, it gave higher current response than CNT/ITO and ITO electrodes. In addition to the conductive nature of Fe_3O_4 nanoparticles and facile electronic nature of MWCNT, the self-perpetuating ionic interaction existing between Fe_3O_4 nanoparticles and MWCNT led to an enhanced charge transport. The ratio of peak oxidation and reduction currents (I_a/I_b), was estimated to be 1.1 for CNT–Fe_3O_4/ITO electrode and 1.3 for CNT/ITO electrode. This pointed out the quasi-reversible nature of the redox processes. In the measured peak currents, maximum current (804.2 μA) was observed for the FDH/CNT–Fe_3O_4/ITO electrode than other electrodes.

Large active surface area of the nanocomposite led to proper immobilization of the FDH enzyme, and ultimately resulted in the large current response of FDH/CNT–Fe_3O_4/ITO electrode. Afterwards as electrodes were coated with BSA protein layer, a fall in peak current of bioelectrodes (741.4 μA) was observed due to blockage of non specific binding sites on the surface of electrode.

Further, the surface coverage of BSA/FDH/CNT/ITO and BSA/FDH/CNT–Fe_3O_4/ITO bioelectrodes was calculated using the Brown-Anson model (Brown and Anson 1977),

$$I_P = \frac{N^2F^2SAV}{4RT} \tag{1}$$

where I_P corresponds to the peak oxidation current in amperes (A), N denotes the number of charge carriers transported, F stands for Faraday's constant (96,485.5 C/mol), S denotes the electrode surface concentration (mol/cm^2), A represents electrode surface area, R stands for the gas constant (8.314 J/K mol), V represents constant scan rate (V/s), and T stands for room temperature (298 K). Using Eq. (1), the surface concentrations of both material bioelectrodes were calculated to be 12.10×10^{-9} mol/cm^2 and 15.79×10^{-9} mol/cm^2, respectively. The diffusivity was calculated using Randles–Sevcik equation,

$$I_P = \left[2.69 \times 10^5\right] AS\sqrt{n^3DV} \tag{2}$$

where I_P stands for peak oxidation current in amperes, n is electron stoichiometry, D stands for diffusion coefficient (cm^2/s), S is the concentration (mol/cm^2), and V stands for scan rate (V/s). For ITO, CNT/ITO, CNT–Fe_3O_4/ITO and BSA/FDH/CNT–Fe_3O_4/ITO electrodes the diffusion coefficients obtained were 1.26×10^{-2}cm^2 s^{-1}, 1.37×10^{-2} cm^2 s^{-1}, 1.50×10^{-2} cm^2 s^{-1}, 1.57×10^{-2} cm^2 s^{-1} respectively. The CV studies of CNT/ITO, CNT–Fe_3O_4/ITO electrodes and BSA/FDH/CNT/ITO, BSA/FDH/CNT–Fe_3O_4/ITO bioelectrodes were explored in PBS at pH 7.4 involving $[Fe(CN)_6]^{3-/4-}$ ion couple at optimized scanning rate (50 mV/s). Fig. S3a and 3b shows the scan rate (10–100 mV/s) studies of bioelectrodes represented by respective cyclic voltammograms (CVs). It was found that the peak current of the redox species increased linearly with respect to square root of scan rate (Mphuthi et al. 2017).

The electrochemical process occurring in the cell was diffusion controlled as indicated by shifting of anodic and cathodic peaks towards higher positive and higher negative potentials respectively. The obtained slopes and intercepts for BSA/FDH/CNT–Fe_3O_4/ITO bioelectrodes were estimated as,

$$I_a = 66.45(\mu A) + [94.27 \times 10^{-6}(A^2\ mV^{-1}\ s)^{\frac{1}{2}} \times \sqrt{scan\ rate(mV\ s^{-1})}];\ (R^2 = 0.998) \tag{3}$$

$$I_c = -154.9(\mu A) - \left[65.3 \times 10^{-6}(A^2\ mV^{-1}\ s)^{\frac{1}{2}} \times \sqrt{scan\ rate(mV\ s^{-1})}\right];\ (R^2 = 0.989) \tag{4}$$

$$V_a = 0.253(V) + \left[0.0183(V)(mV^{-1}\ s)^{\frac{1}{2}} \times \sqrt{\text{scan rate}(mV\ s^{-1})}\right];\ (R^2 = 0.995) \tag{5}$$

$$V_c = 0.0893(V) - \left[0.0173(V)(mV^{-1}\ s)^{\frac{1}{2}} \times \sqrt{scan\ rate(mV\ s^{-1})}\right];\ (R^2 = 0.986) \tag{6}$$

Using Eqs. (5) and (6) the peak potentials for anode (V_a) and cathode (V_c) were found to be 0.3824 V and − 0.0309 V respectively at fixed scan rate (50 mV s^{-1}). While the corresponding anodic (I_a) and cathodic currents (I_c) calculated using Eqs. (3) and (4) were found to be 732.9 μA and − 616.6 μA. In order to further investigate the properties of interfacial electrical double layer arising due to interaction of biomolecules with the electrode, electrochemical impedance studies of various electrodes were conducted. The charge transfer dynamics were also explored by studying Nyquist plots of the electrochemical impedance data.

Impedance spectroscopy of ITO, CNT/ITO, CNT–Fe_3O_4/ITO and FDH/CNT–Fe_3O_4/ITO electrodes was studied in PBS, pH 7.4, containing 5 mM $[Fe(CN)_6]^{3-/4-}$ redox couple at a fixed biasing voltage of 0.25 V in the

frequency range 0.01–10^4 Hz. Nyquist plots for ITO, CNT/ITO, CNT–Fe_3O_4/ITO and FDH/CNT–Fe_3O_4/ITO electrodes were plotted (Fig S4b). The charge transfer resistance (R_{ct}) for CNT/ITO and CNT–Fe_3O_4/ITO electrodes was found to be 456.9 Ω and 378.8 Ω, respectively. The decrease in charge transfer resistance for CNT–Fe_3O_4/ITO electrode as compared to CNT/ITO was may be due to hindrance caused to the transport of charge across the interface of the CNT–Fe_3O_4 composite. After immobilization of enzyme onto CNT–Fe_3O_4/ITO, the R_{ct} value further decreased to 334.9 Ω indicating successful modification of CNT–Fe_3O_4/ITO surface with enzyme. This decrease in impedance might be perhaps due to parallel orientation of enzyme with the nanocomposite structure resulting in enhanced electron conduction towards the electrode while due to incorporation of BSA molecules, the R_{ct} value increased (by threefold, 345 Ω) due to hindrance of steric bulk generated in $K_3[Fe(CN)_6]/K_4[Fe(CN)_6]$ redox reaction. Heterogeneous electron transfer rate constant (K_e) was calculated for ITO, CNT/ITO, CNT–Fe_3O_4/ITO and FDH/CNT–Fe_3O_4/ITO electrodes by using following equation,

$$K_e = \frac{RT}{n^2F^2AR_{CT}S} \tag{7}$$

where R stands for gas constant (8.314 J/K mol), T stands for absolute temperature (K), F is the Faraday's constant (C mol^{-1}), A is electrode surface area (cm^2), the bulk solution concentration (mol cm^{-3}) is denoted by S, n stands for constant denoting number of electron transferred in electrochemical reaction. As calculated constants (K_e) for ITO, CNT/ITO, CNT–Fe_3O_4/ITO and BSA/FDH/CNT–Fe_3O_4/ITO electrodes were found to be 1.09×10^{-5} cm/s, 1.16×10^{-5} cm/s, 1.39×10^{-5} cm/s and 1.54×10^{-5} cm/s, respectively. The highest electron transfer rate constant for BSA coated bioelectrode indicated that the complex structure formed through binding of enzyme with nanocomposite onto ITO promoted faster electron transport via reduction of resistive hindrance (Dhyani et al. 2012).

The relation among the frequency for maximum impedance (f_m), time constant (τ), electron transfer resistance (R_{ct}) and capacitance (C_{dl}) of the interfacial double layer is given by the equation,

$$R_{ct}C_{dl} = \frac{1}{2\pi f_m} = \tau \tag{8}$$

The time constants (τ) for ITO, CNT/ITO, CNT–Fe_3O_4/ITO, FDH/CNT–Fe_3O_4/ITO and BSA/FDH/CNT–Fe_3O_4/ITO electrodes were found to be 0.002 s, 0.012 s, 0.004 s, 0.008 and 0.015 s, respectively. The time constant for BSA/FDH/CNT–Fe_3O_4/ITO bioelectrode was found higher than FDH/CNT–Fe_3O_4/ITO electrode owing to sluggish movement of $[Fe(CN)_6]^{3-/4-}$ ions across the enzyme electrode layer/solution interfacial layer. The large time constant obtained for CNT/ITO compared to CNT–Fe_3O_4/ITO electrode might be perhaps due to variation of time constant with the diffusitivity of ions as there might be variations in interfacial double layer capacitance arising because of redox species present in electrolyte solution.

Electrochemical detection of formaldehyde

The biosensing response of BSA/FDH/CNT/ITO (control) and BSA/FDH/CNT–Fe_3O_4/ITO bioelectrodes was investigated by varying concentrations of formaldehyde and using an enzyme, formaldehyde dehydrogenase. The addition of cofactor NAD^+ (0.5 mM) further enhanced the stability of the enzymatic reaction. Figure 4a and 4b illustrates the oxidation and reduction peaks obtained for varying concentrations of formaldehyde in the electrolyte. It was observed that response current for both the bioelectrodes increased as the concentration of formaldehyde was increased. Although, the relative change in current was found to be more pronounced in nanocomposite based bioelectrode. This was probably due to strong affinity of formaldehyde with the formaldehyde dehydrogenase enzyme that promoted spatial orientation and further provided easy conducting route for electron transfer (Noor Aini et al. 2016). The calibration curves were plotted for BSA/FDH/CNT/ITO and BSA/FDH/CNT–Fe_3O_4/ITO bioelectrodes as function of formaldehyde concentration (inset, Fig. 4a and 4b).

From the calibration curves, sensitivities of both control and nanocomposite based electrodes were calculated. It was found that BSA/FDH/CNT–Fe_3O_4/ITO bioelectrode exhibited comparatively higher sensitivity (527 μA mg/L^{-1} cm^{-2}) within detection range (0.05–0.50 mg/L) and it may be credited to excellent electron transfer in electrochemical biosensor. Besides this fabricated nanocomposite based formaldehyde biosensor exhibited higher sensitivity than BSA/FDH/CNT/ITO bioelectrode. We have performed control experiments with both CNT/ITO and CNT–Fe_3O_4/ITO electrodes in PBS with $[Fe(CN)_6]^{3-/4-}$ redox couple using cyclic voltammetry. It was found that the output peak current in the CNT/ITO electrode didn't change significantly with the variation of formaldehyde concentration. However, the sensitivity of BSA/FDH/CNT/ITO bioelectrode was calculated (225.7 μA mg/L^{-1} cm^{-2}) and found that the sensitivity obtained with the nanocomposite electrode (527 μA mg/L^{-1} cm^{-2}) was, however, more than twice than that obtained with control material (CNT).

Limit of detection (LOD) depending upon standard deviation of calibration curve (σ) and sensitivity of biosensor (m) was calculated by using standard formula,

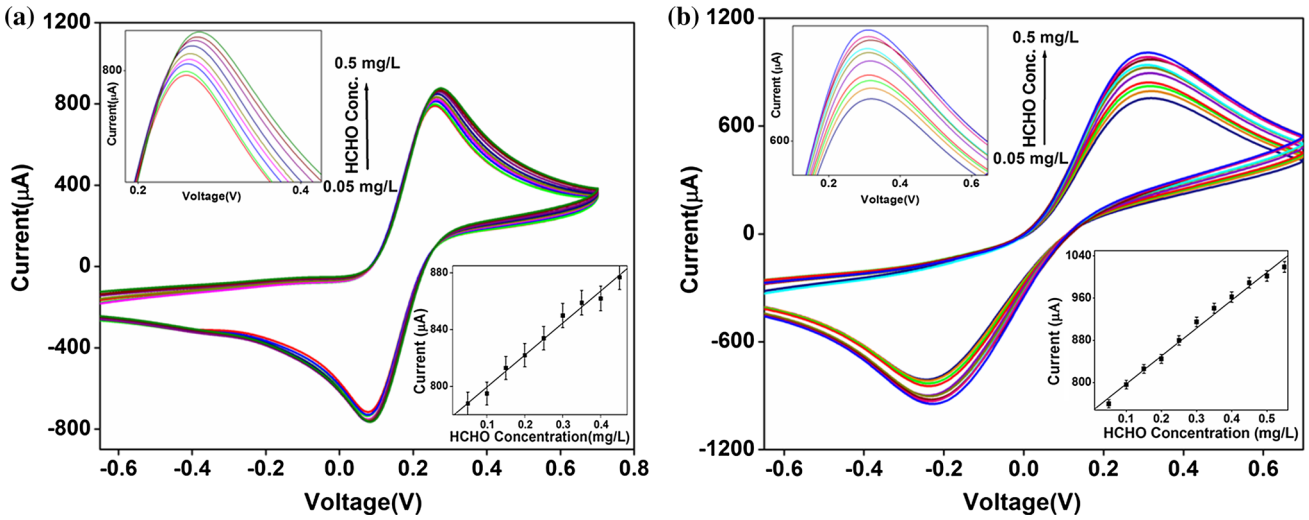

Fig. 4 Cyclic voltammetry studies of **a** BSA/FDH/CNT/ITO and **b** BSA/FDH/CNT–Fe_3O_4/ITO bioelectrodes as a function of formaldehyde concentrations from 0.05–0.50 mg/L, (inset image: a calibration curve of peak current value plotted against formaldehyde concentrations)

$$Detection\ limit = \frac{3\sigma}{m} \quad (9)$$

The calculated LOD for nanocomposite based biosensor was found to be far better than earlier reported studies on formaldehyde biosensors (Table 1). It might be probably due to increased surface to volume ratio in nanocomposite that further enhanced the enzyme loading on to the film. The large surface area and presence of large number of active functional groups on CNT led to high surface to volume ratio in CNT–Fe_3O_4 nanocomposite.

Specificity and stability studies

The presence of possible naturally occurring chemical interferents in the sample and their influence on the biosensor response towards detection of formaldehyde was investigated. In this regard, the intervening effect of chemicals such as alcohols (methanol and ethanol), acetaldehyde, glucose, acetone and formic acid was studied using CV and specificity of nanocomposite based formaldehyde biosensor was evaluated (Ling and Heng 2010). Interferent was added in equal proportion with the formaldehyde (1:1) in PBS (pH 7.4) and the resulting peak current was measured. Current responses obtained with different interferents were measured and their influence on the peak current were calculated using equation,

$$\%Interference = \frac{I_{FD} - I_{int}}{I_{FD}} \quad (10)$$

Negligible interference was found with a maximum of 2.9 and 3.0 in case of acetaldehyde using nanocomposite and controlled bioelectrodes respectively (Fig. S5a and S6a). This showed that FDH enzyme interacts specifically with BSA/FDH/CNT–Fe_3O_4/ITO bioelectrode and this electrode is very much selective for formaldehyde detection. The reproducibility tests of the controlled and nanocomposite bioelectrodes were also conducted using five different bioelectrodes with constant formaldehyde concentration (0.15 mg/L) and constant electrode surface area (Fig. S5b and S6b). Negligible change in the peak current was observed with all the bioelectrodes, as indicated by relative standard deviation (RSD) (0.79%) and average current value (818.8 μA) for BSA/FDH/CNT–

Table 1 Developed biosensors for formaldehyde detection in previous studies and in the present work

Bioelectrode/matrix	Linearity/detection range	Detection limit	Long term stability (days)	Reference
Alcohol oxidase on acryloxysuccinimide-modified acrylic microspheres	0.3–316.2 mM	0.3 mM	48	Ling and Heng (2010)
Carbon electrode modified with chitosan and gold nanoparticles	0.01–10 mg/L	0.1 mg/L	–	Noor Aini et al. (2016)
Carbon electrode modified with polypyrrole and CNT	1–360 mg/L	0.1 mg/L	15	Wang et al. (2012)
FDH/CNT–Fe_3O_4/ITO	0.05–0.50 mg/L	0.05 mg/L	77	Present work

Table 2 Recovery rates of formaldehyde in orange juice using CNT and CNT–Fe_3O_4 biosensors

Formaldehyde added (ppm)	Expected value (ppm)	Measured value (ppm)		Recovery (%)		RSD (%)	
		Extracted juice	Commercial juice	Extracted juice	Commercial juice	Extracted juice	Commercial juice
CNT biosensor							
0.10	0.10	0.095	0.097	95	97	1.43	1.64
0.15	0.15	0.148	0.152	98.6	101	1.56	1.74
0.25	0.25	0.234	0.249	94	97	1.67	1.79
CNT–Fe_3O_4 biosensor							
0.10	0.10	0.099	0.098	99	98.2	0.82	0.95
0.15	0.15	0.157	0.151	104	100	0.89	1.06
0.25	0.25	0.251	0.250	99.9	100	1.13	1.15

Fe_3O_4/ITO bioelectrodes as compared to RSD (1.74%) and average current value (808 μA) for controlled bioelectrode. A comparatively low RSD value obtained for nanocomposite based biosensor implied highly precise fabricated biosensor. Further, the stability of biosensor was studied by measuring the oxidation current response for 0.15 mg/L concentration of formaldehyde at a regular interval of 1 week (Ali et al. 2016). The nanocomposite based bioelectrode was left with about 85% of the initial current response even after 11 weeks when stored at 4 °C; afterwards the current response reduced by 29% (Fig. S5c and S6c), as compared to corresponding fall in current response with controlled bioelectrode as observed after 5 weeks. Thus, the shelf life of the nanocomposite based biosensor was estimated to be as 11 weeks without any significant change of initial current, when bioelectrode is stored in refrigerator (4 °C). This indicated improved shelf life of CNT–Fe_3O_4 nanocomposite biosensor as compared to CNT based biosensor.

Real sample analysis with the developed biosensor

The developed biosensor was used with real samples to validate and prove the diagnostic utility of CNT–Fe_3O_4 biosensor as in previously reported studies (Azizi et al. 2016). Juice extracted from the orange fruits and commercialized orange juice brand available in market were spiked with formaldehyde in the range 0.05 mg/L–0.50 mg/L. The resulting response of CNT and CNT–Fe_3O_4 bioelectrodes was measured and has been reported in Table 2. The relative standard deviations (RSD %) for extracted juice was found to be lower than the commercialized juice for both the bioelectrodes. This was probably due to more interferents present in the commercialized juice. Overall low values of RSD indicated good precision and acceptability of the developed biosensor for testing formaldehyde adulteration in orange juice (Mathias et al. 2014). The recovery rates calculated for both types of juices using controlled bioelectrodes were in the range of 94–101%, while using nanocomposite bioelectrodes were in the range of 98.2–104%. Hence, the nanocomposite based biosensor showed a better recovery rate and is indicative of the accuracy of the method.

Conclusion

The present work demonstrates the development of a novel formaldehyde biosensor for orange juice based on electrochemical sensing. The change in the current signal of biosensor due to complex formation on the surface of controlled and nanocomposite based bioelectrodes was investigated. The resulting sensitivity and long shelf life of electrodes suggest potential future applications of the nanocomposite based biosensor for food quality and safety analysis in agriculture. The nanocomposite (CNT–Fe_3O_4) based biosensor showed good linearity range, high stability, reproducibility, recovery rates $> 90\%$ and RSD $<$ 1.79, indicating the potential of biosensor for selective and precise detection of formaldehyde adulteration in orange juice. Availability of such rapid and on site testing of adulteration will enhance consumer confidence in the safety of food and assist in framing or revising food safety standards and regulations. The aim of sustainable agricultural development can be realized with the interventions of such novel technologies.

Acknowledgements We sincerely express gratitude to Director, CSIR-NPL, New Delhi, India for providing the research facilities and encouragement. We are grateful to Mr. Jai Singh and Mr. Dinesh CSIR-NPL for SEM and TEM measurements respectively. The sponsorship support received from ICAR-IARI, New Delhi, India is gratefully acknowledged.

References

Ahmed KMF, Hafez RS, Morgan SD, Awad AA (2015) Detection of some chemical hazards in milk and some dairy products. Afr J Food Sci 9:187–193

Ali MA, Singh C, Mondal K, Srivastava S, Sharma A, Malhotra BD (2016) Mesoporous few-layer graphene platform for affinity biosensing application. ACS Appl Mater Interfaces 8:7646–7656

Azizi SN, Ghasemi S, Amiripour F (2016) Nickel/P nanozeolite modified electrode: a new sensor for the detection of formaldehyde. Sens Actuator B Chem 227:1–10

Bhardwaj H, Singh C, Kumar Pandey M, Sumana G (2016) Star shaped zinc sulphide quantum dots self-assembled monolayers: preparation and applications in food toxin detection. Sens Actuators B Chem 231:624–633

Brown AP, Anson FC (1977) Cyclic and differential pulse voltammetric behavior of reactants confined to the electrode surface. Anal Chem 49(11):1589–1595. https://doi.org/10.1021/ac50019a033

Das M, Dhand C, Sumana G, Srivastava AK, Nagarajan R, Malhotra BD (2012) Electrophoretically fabricated core-shell CNT-DNA biowires for biosensing. J Mater Chem 22:2727–2732

Dhyani H, Ali MA, Pandey MK, Malhotra BD, Sen P (2012) Electrophoretically deposited CdS quantum dots based electrode for biosensor application. J Mater Chem 22:4970–4976

Ding B, Wang H, Tao S, Wang Y, Qiu J (2016) Preparing electrochemical active hierarchically porous carbons for detecting nitrite in drinkable water. RSC Adv 6:7302–7309

European Food Safety Authority C (2007) Opinion of the scientific panel on food additives, flavourings, processing aids and materials in contact with food (AFC) related to use of formaldehyde as a preservative during the manufacture and preparation of food additives. EFSA 5:415. https://doi.org/10.2903/j.efsa.2007.415

Fayemi OE, Adekunle AS, Ebenso EE (2017) Electrochemical determination of serotonin in urine samples based on metal oxide nanoparticles/MWCNT on modified glassy carbon electrode. Sens Biosens Res 13:17–27

Fischer MJE (2010) Amine coupling through EDC/NHS: a practical approach. Surface Plasmon Resonan Methods Protoc 8:55–73. https://doi.org/10.1007/978-1-60761-670-2_3

Goon S, Bipasha M, Islam MS, Hossain MB (2014) Fish marketing status with formalin treatment in bangladesh. IJPHS3:95-100. ISSN:2252-8806. https://media.neliti.com/media/publications/7179-EN-fish-marketing-status-with-formalin-treatment-in-bangladesh.pdf

Han R, Li W, Pan W, Zhu M, Zhou D, Li F-s (2014) 1D magnetic materials of Fe_3O_4 and Fe with high performance of microwave absorption fabricated by electrospinning method. Sci Rep 4. https://doi.org/10.1038/srep07493

Hariani PL, Faizal M, Setiabudidaya D (2013) Synthesis and properties of Fe_3O_4 nanoparticles by co-precipitation method to removal procion dye. IJESD 4:336. ISSN: 2010-0264. http://eprints.unsri.ac.id/id/eprint/2708

Jeong H-S, Chung H, Song S-H, Kim C-I, Lee J-G, Kim Y-S (2015) Validation and determination of the contents of acetaldehyde and formaldehyde in foods. Toxicol Res 31:273

Kang YS, Risbud S, Rabolt JF, Stroeve P (1996) Synthesis and characterization of nanometer-size Fe_3O_4 and Y-Fe_2O_3 particles. Chem Mater 8:2209–2211

Khataee A, Lotfi R, Hasanzadeh A, Iranifam M (2016) A simple and sensitive flow injection method based on the catalytic activity of CdS quantum dots in an acidic permanganate chemiluminescence system for determination of formaldehyde in water and wastewater. Photochem Photobiol Sci 15:496–505

Korpan YI, Gonchar MV, Sibirny AA, Martelet C, El'skaya AV, Gibson TD, Soldatkin AP (2000) Development of highly selective and stable potentiometric sensors for formaldehyde determination. Biosens Bioelectron 15:77–83

Kulkarni SA, Sawadh PS, Palei PK, Kokate KK (2014) Effect of synthesis route on the structural, optical and magnetic properties of Fe_3O_4 nanoparticles. Ceram Int 40:1945–1949

Kumar A, Goyal SK, Pradhan RC, Goyal RK (2015) A study on status of milk adulterants using in milk of district Varanasi. South Asian J Food Technol Environ 1:140–143. ISSN: 2394-5168(Print),2454-6445 (online). http://www.sweft.in/download/volumes1_:_issue_2__/Paper%207.pdf

Ling YP, Heng LY (2010) A potentiometric formaldehyde biosensor based on immobilization of alcohol oxidase on acryloxysuccinimide-modified acrylic microspheres. Sensors 10:9963–9981. https://doi.org/10.3390/s101109963

Mabood F, Hussain J, Al Nabhani MMO, Gilani SA (2017) Detection and quantification of formalin adulteration in cow milk using near infrared spectroscopy combined with multivariate analysis. J Adv Dairy Res 5:2

Mathias PC, Hayden JA, Laha TJ, Hoofnagle AN (2014) Evaluation of matrix effects using a spike recovery approach in a dilute-and-inject liquid chromatography-tandem mass spectrometry opioid monitoring assay. Clin Chim Acta 437:38–42

Mphuthi NG, Adekunle AS, Fayemi OE, Olasunkanmi LO, Ebenso EE (2017) Phthalocyanine doped metal oxide nanoparticles on multiwalled carbon nanotubes platform for the detection of dopamine. Sci Rep 7. https://doi.org/10.1038/srep43181

Nedellec V, Rabl A, Dab W (2016) Public health and chronic low chlordecone exposure in Guadeloupe, part 1: hazards, exposure-response functions, and exposures. Environ Health 15:75

Noor Aini B, Siddiquee S, Ampon K (2016) Development of formaldehyde biosensor for determination of formalin in fish samples; malabar red snapper (*Lutjanus malabaricus*) and longtail tuna (*Thunnus tonggol*). Biosensors 6:32. https://doi.org/10.3390/bios6030032

Paul Joseph D, Venkateswaran C, Selva Vennila R (2010) Critical analysis on the structural and magnetic properties of bulk and nanocrystalline Cu–Fe–O. Adv Mater Sci Eng. https://doi.org/10.1155/2010/715872

Pramod P, Joseph STS, Thomas KG (2007) Preferential end functionalization of Au nanorods through electrostatic interactions. J Am Chem Soc 129:6712–6713

Razzino CA, Sgobbi LF, Canevari TC, Cancino J, Machado SAS (2015) Sensitive determination of carbendazim in orange juice by electrode modified with hybrid material. Food Chem 170:360–365

Sharma R et al (2013) Phase control of nanostructured iron oxide for application to biosensor. J Mater Chem B 1:464–474

Sherman DM, Waite TD (1985) Electronic spectra of Fe^{3+} oxides and oxide hydroxides in the near IR to near UV. Am Miner 70:1262–1269

Singh C et al (2013) Carboxylated multiwalled carbon nanotubes based biosensor for aflatoxin detection. Sens Actuators B Chem 185:258–264

Wahed P, Razzaq MA, Dharmapuri S, Corrales M (2016) Determination of formaldehyde in food and feed by an in-house validated HPLC method. Food Chem 202:476–483

Wang M, Jiang S, Chen Y, Chen X, Zhao L, Zhang J et al (2012) Formaldehyde biosensor with formaldehyde dehydrogenase adsorped on carbon electrode modified with polypyrrole and carbon nanotube. Engineering 4(10):135. https://doi.org/10.4236/eng.2012.410B035

World Health O (2004) IARC monographs on the evaluation of carcinogenic risks to humans. Volume 88: formaldehyde,

2-butoxyethanol and 1-tert-butoxypropan-2-ol, vol 88. WHO, Geneva, Switzerland. ISBN: 9283212886

Zhang X et al (2015) Studies on the determination of formaldehyde in squid and bummalo. AER 46:20–22. file:///C:/Users/asus/Downloads/25846129%20(1).pdf

Zhu X, Liu M, Liu Y, Chen R, Nie Z, Li J, Yao S (2016) Carbon-coated hollow mesoporous FeP microcubes: an efficient and stable electrocatalyst for hydrogen evolution. J Mater Chem A 4:8974–8977